





Layered gallium sulfide optical properties from monolayer to CVD crystalline thin films

Yael Gutiérrez,^{1,7}  Dilson Juan,² Stefano Dicorato,¹ Gonzalo Santos,² Matthias Duwe,³ Peter H. Thiesen,³ Maria M. Giangregorio,¹ Fabio Palumbo,¹ Kurt Hingerl,⁴ Christoph Cobet,⁴ Pablo García-Fernández,⁵ Javier Junquera,⁵ Fernando Moreno,²  and Maria Losurdo^{6,8}

¹Institute of Nanotechnology, CNR-NANOTEC, c/o Department of Chemistry, Università degli Studi di Bari, Via Orabona 4, 70126 Bari, Italy

²Departamento de Física Aplicada, Universidad de Cantabria, Avda. de los Castros s/n 39005, Santander, Spain

³Accurion GmbH, Stresemannstraße 30, D-37079 Göttingen, Germany

⁴Center for Surface and Nanoanalytics (ZONA), Johannes Kepler Universität, A-4040 Linz, Austria

⁵Departamento de Ciencias de la Tierra y Física de la Materia Condensada, Universidad de Cantabria, Cantabria Campus Internacional, Avda. de los Castros s/n 39005 Santander, Spain

⁶Istituto di Chimica della Materia Condensata e delle Tecnologie per l'Energia, CNR-ICMATE, C.so Stati Uniti 4, 35127 Padova, Italy

⁷yael.gutierrezvela@nanotec.cnr.it

⁸maria.losurdo@cnr.it

Abstract: Interest in layered van der Waals semiconductor gallium monosulfide (GaS) is growing rapidly because of its wide band gap value between those of two-dimensional transition metal dichalcogenides and of insulating layered materials such as hexagonal boron nitride. For the design of envisaged optoelectronic, photocatalytic and photonic applications of GaS, the knowledge of its dielectric function is fundamental. Here we present a combined theoretical and experimental investigation of the dielectric function of crystalline *2H*-GaS from monolayer to bulk. Spectroscopic imaging ellipsometry with micron resolution measurements are corroborated by first principle calculations of the electronic structure and dielectric function. We further demonstrate and validate the applicability of the established dielectric function to the analysis of the optical response of *c*-axis oriented GaS layers grown by chemical vapor deposition (CVD). These optical results can guide the design of novel, to our knowledge, optoelectronic and photonic devices based on low-dimensional GaS.

© 2022 Optica Publishing Group under the terms of the [Optica Open Access Publishing Agreement](#)

1. Introduction

In the last few years group-III monochalcogenides such as gallium sulfide, GaS, [1–3] gallium selenide, GaSe [2,4] and gallium telluride, GaTe [5,6], have attracted increasing attention. These van der Waals (vdW) layered semiconductors consists of a stacking along the *c*-axis of covalently bonded tetralayers (X-Ga-Ga-X, X = S, Se, Te) held together by vdW forces (see Fig. 1). Their energy band gap values, E_g , span the visible range, with GaTe ($E_g \approx 1.7$ eV) [5] < GaSe ($E_g \approx 2.0$ eV) [7] < GaS ($E_g \approx 2.3 - 2.6$ eV [8–13]) to values higher than 3 eV for monolayers, being between the two-dimensional (2D) transition metal dichalcogenides (TMDs) and insulating materials such as hexagonal boron nitride (h-BN) [3], as shown in Fig. 1.

Among those, low-dimensional layered GaS is of special interest because its bandgap has been predicted to increase from the bulk value of $E_g \approx 2.3 - 2.6$ eV to $E_g \approx 3.2$ eV for the monolayer. [14–16] Indeed, the wide band gap of layered GaS has been already exploited in a variety

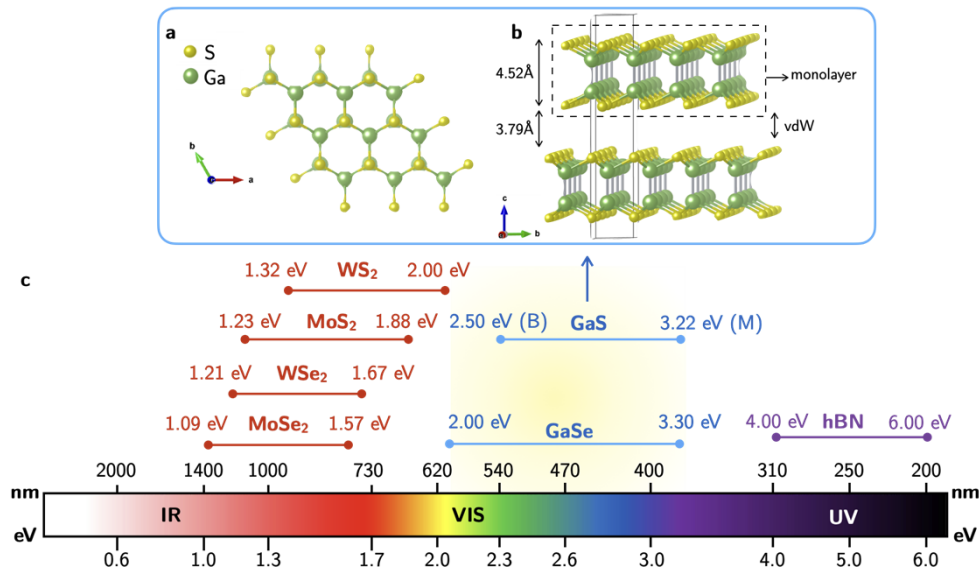


Fig. 1. (a) Side and (b) top view of the crystalline structure of 2H-GaS. (c) Positioning of Ga-monochalcogenides GaS and GaSe in the bandgap energy space of two-dimensional semiconductors, with their corresponding band-gap energies for the bulk (left value of the bar) and for the monolayer (right value of the bar).

of optoelectronic applications spanning from transistors [17] and visible-UV photodetectors, [1,18–21] and to energy storage, gas sensing, and photocatalysis [1,22–24].

Despite the exploited applications, optical properties of layered GaS are still widely scattered. For instance, only two experimental contradicting profiles can be found in literature for the dielectric function of bulk GaS, [12,25] while, to the best of our knowledge, the dielectric function of low-dimensional GaS and its dependence on the number of layers is still uninvestigated.

Here we assess the dielectric function of GaS, from bulk down to monolayer, by a combined theoretical and experimental investigation. Imaging spectroscopic ellipsometry measurements of the dielectric function of bulk *c*-axis cleaved single crystal 2H-GaS and of mechanically exfoliated monolayer and few-layers have been correlated with density of states and band diagrams, and dielectric function calculated by first principles methods in the framework of density functional theory (DFT). Our calculations and experimental results demonstrate that for monolayers and few layers GaS mainly the in-plane component, which is almost independent of the number of layers, defines the dielectric function. From the assignment of the Ga and S orbitals contributing to the interband electronic transitions and associated critical points (CPs), the interlayer vdW interaction due to chalcogenide S-electrons contributes to the out-of-plane component. A blue-shift of the fundamental indirect bandgap is found both experimentally and by theory from 2.6 eV for bulk to approximately 2.7 eV for about 5 layers and extrapolated to 3.1 eV for monolayer. We also demonstrate the applicability of the determined dielectric function to analyze extensively and quantitatively the optical response of polycrystalline GaS layers deposited by chemical vapor deposition (CVD).

Thus, our results on the GaS optical properties provide a solid foundation to the design of photonic, optoelectronic and photocatalytic applications of low-dimensional GaS.

2. Methods

2.1. GaS layers preparation

Mechanically exfoliated GaS flakes were obtained using a standard thermal tape method on a hotplate set at 90°C by 2H-GaS *c*-axis oriented bulk crystals purchased from 2D semiconductors and HQ graphene. Epitaxial quality *c*-plane sapphire (0001) with a surface roughness (RMS = root mean surface roughness) of 0.2 nm was used as substrate. Further details about exfoliated layers can be found in Refs. [21,26]

Crystalline GaS layers were also grown using chemical vapor deposition (CVD) on sapphire at 650°C using Ga₂S₃ as precursor (kept at a temperature of 800°C) and H₂ as carrier gas at a pressure of 100 mbar.

2.2. GaS layers characterization

The exfoliated and CVD layers were characterized chemically, structurally, and morphologically by a combination of techniques.

All the samples analyzed here (i.e., bulk exfoliated and CVD) had a chemical composition of Ga/S = 1.0 ± 0.1 as revealed by X-ray photoelectron spectroscopy (XPS). XPS measurements were carried out by a Scanning XPS Microprobe (PHI 5000 Versa Probe II, Physical Electronics) equipped with a monochromatic Al K α X-ray source (1,486.6 eV), with a spot size of 200 μ m. Survey (0–1,200 eV) and high-resolution spectra (C1s, O1s, S2p, S2s, Ga2p3, Ga3d) were recorded in FAT mode at a pass energy of 117.40 and 29.35 eV, respectively. Spectra were acquired at a take-off angle of 45° with respect to the sample surface. Surface charging was compensated using a dual beam charge neutralization system, and the hydrocarbon component of C1s spectrum was used as internal standard for charging correction, and it was fixed at 285.

The crystalline quality after exfoliation was checked by X-ray diffraction (XRD) in thin film geometry. The measurements were performed with an Ultima IV diffractometer (Rigaku Corp., Japan), equipped with parallel beam optics and a thin film attachment, using Cu K α radiation (λ = 1.5405 Å), operated at 30 mA and 40 kV, over the 2 θ range 5–70°, at a scanning rate of 1°/min, with a step width of 0.02°.

Raman spectroscopy was performed with a LabRam Horiba using a 532 nm wavelength laser (20 mW) with a \times 100 microscope objective (NA = 0.9).

Morphology and thickness of ultrathin layers were determined by atomic force microscopy (AFM) using the Autoprobe CP (Thermomicroscope). The sample topography was recorded in a single-pass mode using a gold-coated Si tip (their frequency is ~80 Hz) in non-contact mode.

Scanning electron microscopy (SEM) was carried out for the morphological characterization of the samples with a Zeiss Supra 219 40 FEG SEM equipped with a Gemini field emission gun. Analyses were carried out at an extraction voltage of 3 kV and 221 a 30- μ m aperture.

In order to validate the derived bulk dielectric function, the same samples were measured with various ellipsometers, namely UVISEL (Horiba), Wollam VASE M2000 Ellipsometer varying the angle of incidence from 50° to 70°, in the photon energy range 0.75–6.5 eV, and with the spectroscopic imaging ellipsometer EP4 (Accurion GmbH, Göttingen) in the spectral range 1.5 - 5 eV, with the angle of incidence set at 50°. All sets of data were modelled with the same model consisting of substrate/GaS/surface/air. The substrate sapphire was experimentally measured before the GaS transfer. The GaS was modelled by a dispersion equation consisting of an ensemble of Tauc-Lorenz (for the E₀ bandgap determination) and Lorentzian oscillators for the higher interband transitions and critical points (E₁-E₆). The surface layer was modelled by a 2 Å thick oscillator (fixed by the AFM).

2.3. First principles calculations

Density functional theory first principles calculations based on a numerical atomic orbital method were carried out using the SIESTA code [27]. All the calculations were performed with the generalized gradient approximation (GGA), using the revised exchange-correlation potential parameterized by Perdew–Burke–Ernzerhof (PBEsol) [28] to simulate the electronic exchange and correlation. Core electrons are described by *ab initio* optimized norm conserving pseudopotentials, generated following the recipe given by Hamann, [29] available in the PSEUDODOJO [30] in the Kleinman–Bylander fully nonlocal separable representation. The 3s, 3p, 3d, 4s, and 4p were considered as valence electrons of Ga and explicitly included in the calculations. For S, as valence electrons, 3s, 3p, and 3d were chosen.

The one-electron Kohn Sham eigenvectors were expanded in a basis of localized numeric atomic orbitals (NAO) as implemented in the SIESTA code. The size of the basis set chosen for Ga was single ζ for the semicore 3s, 3p and 3d; double ζ for 4s, 4p and 4d polarization orbital. The size of the basis set chosen for S was double ζ for 3s, 3p and 3d orbitals, in all cases with default cutoff radii. The electronic density, Hartree, and exchange correlation potentials, as well as the corresponding matrix elements between the basis orbitals, were calculated in a uniform real space grid. The equivalent plane wave cut-off used to represent the charge density was 1200 Ry. For the Brillouin zone integrations, a Monkhorst–Pack [31] sampling of $15 \times 15 \times 3$ was used for the bulk phases and $20 \times 20 \times 1$ for the slabs representing mono-, bi- and tri-layers. For the 2H-bulk structure computation, atoms and unit cell were allowed to relax until the maximum component of the force acting on any atom was smaller than 0.01 eV \AA^{-1} , and the maximum component of the stress was 0.1 GPa. For determining the slabs unit cell parameters, we started from the equilibrium lattice parameters of bulk calculations and the atoms were allowed to relax only in the x - y plane perpendicular to the c direction.

2.4. Optical response

The frequency dependent optical response of the studied structures was obtained using first-order time-dependent perturbation theory to calculate the dipolar transition matrix elements between occupied and unoccupied single-electron eigenstates as implemented in the SIESTA code. The optical constants of a solid can be derived from the complex dielectric function $\epsilon(\omega) = \epsilon_1(\omega) + i\epsilon_2(\omega)$. The frequency-dependent dielectric function can be written within the dipole approximation as

$$\epsilon_2(\omega) = \frac{2\pi}{mN} \frac{\omega_p^2}{\omega^2} \sum_{v,c} \int_{\text{BZ}} \frac{dk}{(2\pi)^3} |M_{cvk}|^2 \delta(\epsilon_{ck} - \epsilon_{vk} - \hbar\omega)$$

where m is the electron mass, N is the number of electrons per unit volume, and $\omega_p^2 = 4\pi Ne^2/m$ is the plasma frequency, with e being the electron charge. The single particle electronic states $|\psi\rangle$ of energy ϵ are labeled by their crystal momentum k and their valence (v) and conduction (c) band index. The sum is over connecting valence and conduction states and over all the k points in the first Brillouin zone. The optical matrix element is given by $M_{cvk} = \langle \psi_{ck} | \hat{e} \cdot \mathbf{p} | \psi_{vk} \rangle$, where \hat{e} is the polarization of the incident light and \mathbf{p} is the momentum operator. The real part of the dielectric function $\epsilon_1(\omega)$ can be obtained from the imaginary part using the Kramers-Kronig relation.

In order to analyze the origin of the peaks appearing in the $\epsilon_2(\omega)$ spectra due to interband transitions, we have calculated the values of the optical matrix element M_{cvk} for every pair of conduction and valence bands at each k point with an energy difference equal to the photon energy at which the peak appear. In this way, we can analyze the pair of bands contributing to the interband transition visible in $\epsilon_2(\omega)$ spectra. All bands have been included in the optical calculations. The optical mesh used for is $38 \times 38 \times 12$ for the bulk and low dimension phases.

The gaussian broadening has been set to 0.3 Ry. In plane optical response was calculated using the unpolarized type, which consider the light propagation vector parallel to c -axis and perpendicular components of the electric field are averaged over the other spatial directions.

3. Results

3.1. GaS crystalline and electronic structure

The GaS phase stable at room temperature and atmospheric pressure is the $2H$ hexagonal lattice with space group $P6_3/mmc$ (no. 194) schematized in Figs. 1(a),(b). It can be mechanically [23,32] and chemically exfoliated [22] down to a monolayer that belongs to the space group $P\bar{6}m2$ (no 187), entering the blooming 2D materials family. Figure 2(a) shows typical SEM images of GaS exfoliated samples down to monolayer, clearly showing the layered structure of the exfoliated crystalline samples analyzed herein. Figure 2(b) shows the scheme as well as lattice parameters and atomic coordinates of $2H$ -bulk GaS primitive unit cell used in the calculations. Interestingly, the DFT calculations revealed that the monolayer and few-layer GaS retains the same unit cells parameters of the bulk (reported in Fig. 2(b)), indicating that the vdW stacking of layers does not affect the in-plane atoms arrangement. This is an important point to consider and explain the independence of in-plane structural and electronic properties of number of layers. Specifically, the optimized crystal lattice constant a obtained by our DFT calculations is 3.541 Å for both the $2H$ -bulk and monolayer; c is 16.616 Å; the Ga–Ga and Ga–S bond lengths are, respectively, 2.35 Å and 2.31 Å, resulting in the S-Ga-Ga-S thickness of 4.52 Å, with an interlayer distance of 3.79 Å. Figures 2(d)-(g) show the calculated electronic band structure density of states (DOS) and projected density of states (PDOS) indicating the contribution of the Ga $4s$, Ga $4p$, S $3s$ and S $3p$ for the monolayer, bilayer, trilayer and bulk GaS. The calculations have been performed using density functional theory (DFT) as implemented in SIESTA [27] (see Methods) and minimizing the energy with standard conjugate-gradient techniques. For the mono-, bi- and tri-layers the calculated electronic structures fail to describe a Mexican hat-type dispersion, which can be observed as a double-peak feature around the Γ -point and previously reported by other authors, [33,34] giving a rather flat band around Γ instead. The aforementioned effect is relatively subtle, and we do not consider that it will affect the optical response of the system; nevertheless, by employing a more complete basis set the feature is recovered.

The band diagrams reveal that bulk as well as monolayer GaS are indirect band gap semiconductors as their valence band maximum (VBM) is located at Γ while their conduction band minimum (CBM) lies at the M point (K for few layers). Furthermore, due to band ordering along the c -axis, the calculated indirect bandgap energy increases going from GaS bulk to monolayer, being 1.96 eV for bulk, 2.11 eV for trilayer, 2.21 eV for bilayer and 2.47 eV for GaS monolayer as shown in Fig. 2(c). Similarly, the direct bandgap increases from 3.51 eV for bulk to 3.66 eV for trilayer, to 3.77 eV for bilayer and to 3.93 eV for monolayer. This increase in the bandgap with the decrease in the number of layers is in good agreement with other calculated values using the same functional, i.e., the PBEsol, [35] although it is known that DFT systematically underestimates the value of the bandgap with semi-local exchange-correlation functionals.

3.2. GaS dielectric function from bulk crystal to monolayer

Figure 3(a) shows the real, ϵ_1 , and imaginary, ϵ_2 , part of the complex dielectric function, $\epsilon(\omega) = \epsilon_1(\omega) + i\epsilon_2(\omega)$, derived under the isotropic assumption modelling of experimental ellipsometric spectra for a $2H$ -GaS bulk single crystal cleaved along the c -axis. The crystal has been qualified structurally by XRD, that showed only the (004), (006), (008) and (010) reflections and by the Raman spectrum (shown in Fig. 5(e)) characterized by the characteristic A_{1g}^1 , E_{2g}^1 and A_{1g}^2 Raman modes of GaS [36] at 187, 293 and 359 cm^{-1} and with an intensity ratio $A_{1g}^1/A_{1g}^2 \sim 1$ that we have statistically verified (measuring 100 spectra of single crystal GaS with different Raman

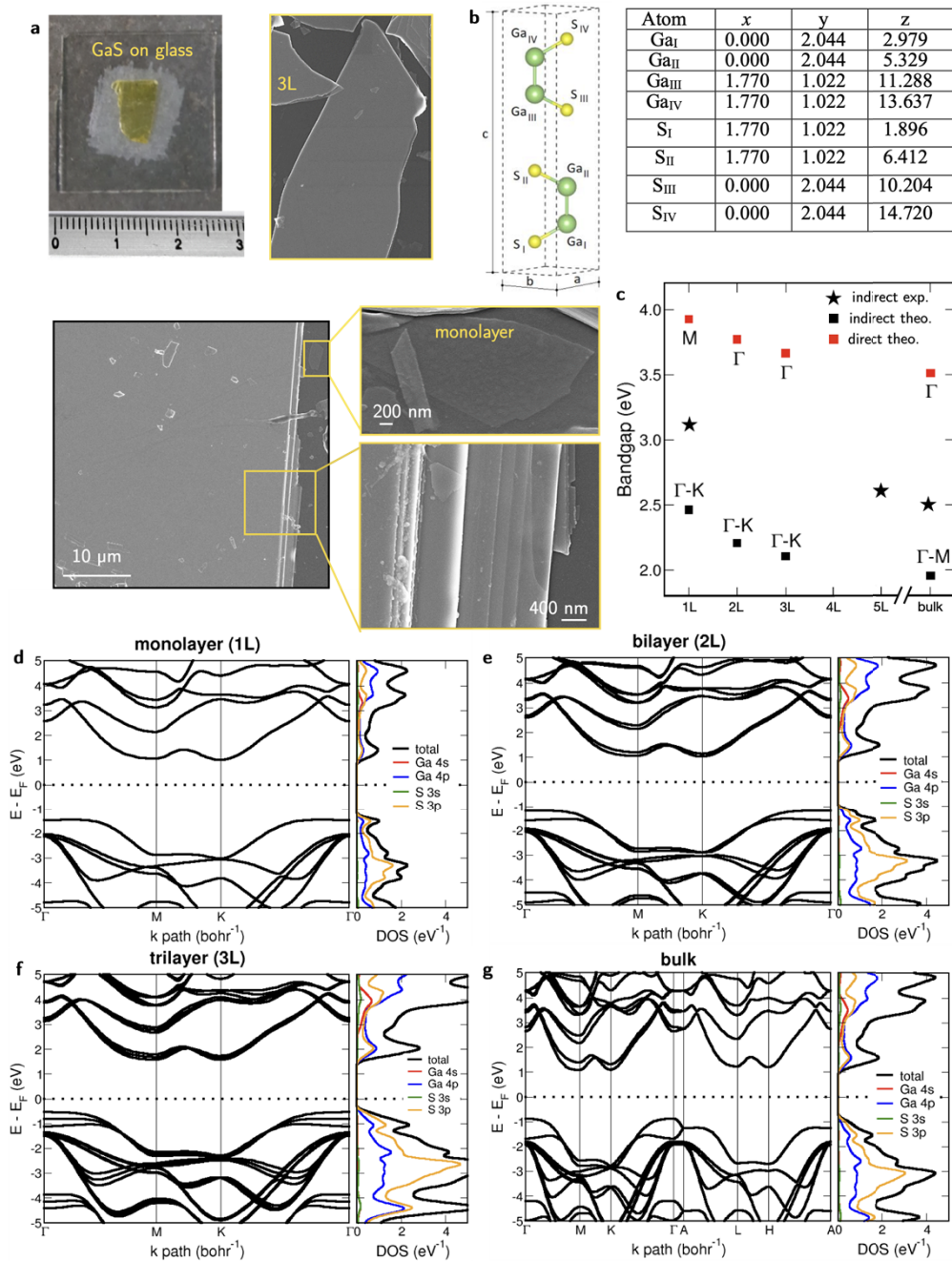


Fig. 2. (a) Picture of cm-scale exfoliated 2H-GaS with SEM views of monolayer, trilayer and multilayer GaS samples. (b) Scheme primitive unit cell of 2H-GaS indicating the lattice parameters as well as atomic coordinates. (c) Calculated indirect and direct (squares) and measured (stars) bandgap energy values depending on the number of GaS layers up to bulk. Calculated electronic band diagram and density of states (DOS) for (d) monolayer, (e) bilayer, (f) trilayer and (g) bulk GaS.

instruments in various laboratories). From the analysis of the ellipsometric spectra, an indirect bandgap energy $E_g = 2.50 \pm 0.05$ eV has been determined for bulk $2H$ -GaS, which agrees well with previously reported bandgap values measured by various methods. [8–13]

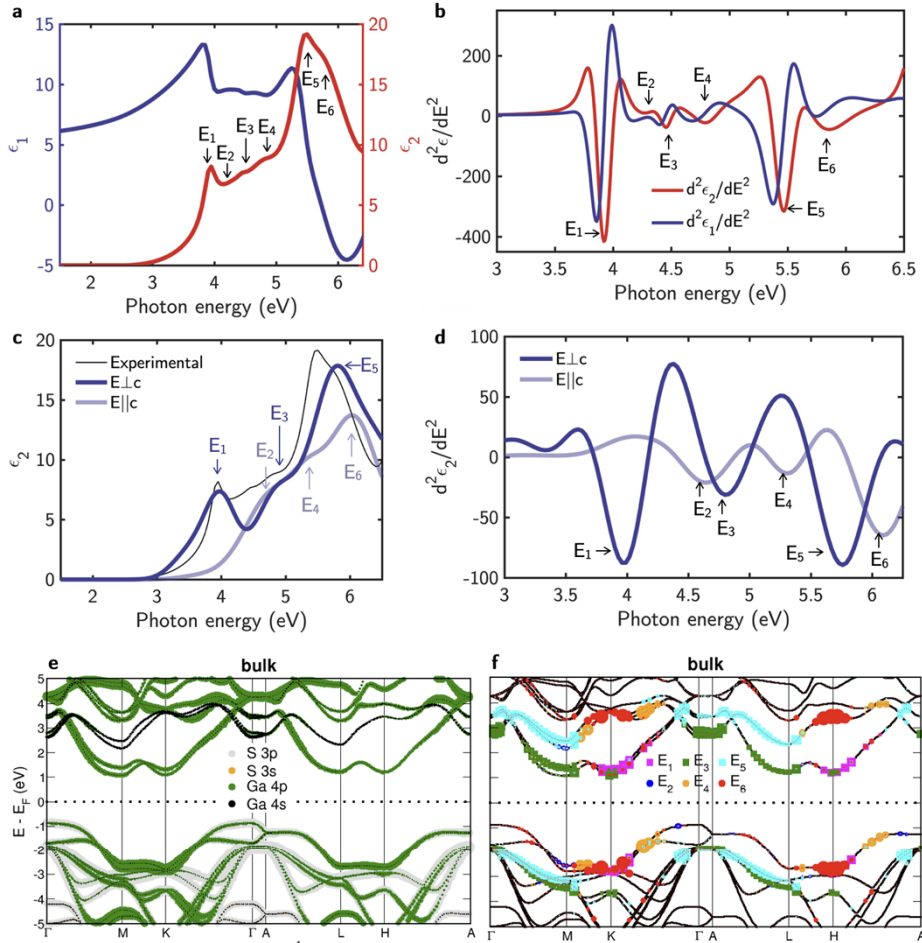


Fig. 3. (a) Real, ϵ_1 and imaginary, ϵ_2 , parts of the complex dielectric function of GaS bulk single crystal. (b) Critical point analysis of the experimentally determined bulk dielectric function by using the second derivative spectra of ϵ_1 and ϵ_2 . The arrows indicate the critical points. (c) Calculated out-of-plane ($E||c$) and in-plane ($E\perp c$) components of the imaginary part of the complex dielectric function of bulk GaS. (d) Critical point analysis of the calculated out-of-plane ($E||c$) and in-plane ($E\perp c$) components of the imaginary part of the complex dielectric function of bulk GaS. (e) Band diagram of GaS representing the contribution of the $S3p$, $S3s$, $Ga4p$ and $Ga4s$ to each band. The size of the marker is proportional to the strength of the orbitals contribution. (f) Band diagram of GaS representing the bands contributing to the interband transitions responsible to the CPs appearing in the dielectric function spectrum.

Based on the band structure and the dipolar transition matrix elements between occupied and unoccupied single-electron eigenstates, the complex dielectric function has been calculated for bulk GaS using first-order time-dependent perturbation theory as implemented in SIESTA [27]. Fig. 3(c) shows the imaginary, ϵ_2 , part of the dielectric function calculated for bulk GaS for the in-plane polarization ($E\perp c$) and out-of-plane polarization ($E||c$). Noteworthy, the calculated

in-plane dielectric function reproduces very well the measured dielectric function, indicating that the in-plane component mostly contributes to the GaS dielectric function, probably because of the weak vdW interactions between stacked layers. Therefore, by the comparison of Fig. 3(a) and Fig. 3(c), we could infer that in the case of GaS, the isotropic assumption in the modelling of the dielectric function mainly results in the in-plane component.

A critical points (CPs) analysis using the second derivative spectra of $\epsilon(\omega)$, $d^2\epsilon_1/dE^2$ and $d^2\epsilon_2/dE^2$, calculated numerically and smoothed using a Savitzky–Golay [38] algorithm reveals several CPs in the experimental $\epsilon(\omega)$ at $E_1 = 3.95$ eV, $E_2 = 4.25$ eV, $E_3 = 4.45$ eV, $E_4 = 4.75$ eV, $E_5 = 5.45$ eV and $E_6 = 5.75$ eV as shown in Fig. 3(b). The details in Table 1 show that the CP energies are in good agreement with those reported in literature [12,25]. Noteworthy, those CPs are well reproduced by the theoretical calculations allowing to distinguish which of them contribute to the in-plane ($\mathbf{E}\perp c$) and out-of-plane ($\mathbf{E}\parallel c$) of the dielectric function. Specifically, the CPs labeled as E_1 , E_3 and E_5 can be assigned to the in-plane ($\mathbf{E}\perp c$) whereas E_2 , E_4 and E_6 can be assigned to the out-of-plane ($\mathbf{E}\parallel c$) component. For the assignment of the CPs, Fig. 3(e) shows the fat bands of bulk GaS representing the contribution of the $S3p$, $S3s$, $Ga4p$ and $Ga4s$ orbitals to each band. The size of the marker is proportional to the strength of the contribution. Therefore, it can be inferred that:

- at M-point, the conduction band minimum (CBM) contains relatively equal anion S $3p$ and cation Ga $4p$ character;
- although at the M, K, L and H boundary zone points in the highest valence band the anion S $3p$ contribution is small in comparison with Ga $4p$, it increases along the lines M- Γ , K- Γ , H-A and L-A to reach maximum values at the center zone Γ and A points;
- the valence band maximum (VBM) at Γ contains a strong, nearly pure S p_z -like charge, in addition to some Ga-Ga antibonding character.

Table 1. Summary of the energy of the main critical points (CPs) as compared to the literature values from Refs. [25,37]

Ref	T (K)	E1 (eV)	E2 (eV)	E3 (eV)	E4 (eV)	E5 (eV)	E6 (eV)
Ref. [25]	300	3.95	4.22	4.51	4.75	5.50	5.78
Ref. [37]	5	4.03	4.30	4.61	4.82	5.57	-
This work experimental	300	3.95	4.25	4.45	4.75	5.45	5.75
in-plane DFT	-	3.95	-	4.8	-	5.75	-
out-of-plane DFT	-	-	4.62	-	5.31	-	6.09

Considering the different contributions of the Ga and S atomic orbitals, the following interband transitions can be assigned to the CPs (see Fig. 3(f)):

- The low-energy peak at 3.95 eV (E_1) corresponds to transitions between the highest valence band and the lowest conduction band in the neighborhood of the high symmetry points K and H in reciprocal space where the bands run parallel. It has a mixed cation Ga- $p_{x,y}$ and anion S- $p_{x,y}$ character as it involves wave functions of both, originating from excitation of the Ga-Ga bond and of non-bonding S- p_z , to s-state transitions.
- The CP at 4.25 eV (E_2) accounts for transitions in the M- Γ line around M between the highest valence band and the conduction band located above approx. 2eV that involves predominantly occupied Ga $4p$ and S $3p$ into empty Ga $4s$ states. High transitions amplitudes appear in the paths T and S between high symmetry points (Γ -K and A-H respectively), corresponding to a sharp feature in the density of state.

- The CP at 4.45 eV (E_3) is assigned to vertical transitions between mixed S $3p$ and Ga $4p$ from the lower lying valence band at ≈ -2 eV around Γ to the pair of lowest conduction bands with Ga $4s$ character. The same occurs between flat bands along the high symmetry path Γ -A. Additional contributions arise along the M- Γ and L-A path involving low lying valence bands around -3 eV and the lowest conduction bands, almost parallel close to M and L, that probably comprise S $3p_z$ and Ga $4p_z$ states. In K and H this excitation replicates involving the same orbitals.
- In the case of the CP at 4.75 eV (E_4) the vertical transitions are out of the high symmetry points and practically located along the center of the M-K- Γ and H-A paths. These transition are associated with S $3p_{x,y}$ to Ga $4s$ orbitals.
- The high energy main peak at 5.45 eV (E_5) corresponds to the CP labeled E_5 that involves mostly transitions associated with S $3p_{x,y}$ to Ga $4s$ orbitals. We find practically continues probabilities along the Γ -M and A-L paths between deeper valence and conduction bands. The peak is reinforced with contributions along T and S.
- Another CP appears at the energy 5.75 eV (E_6) as a shoulder in the main peak. It has important contributions around K and H high symmetry points and minor contributions spread over almost the whole Brillouin zone. Optical transitions involve mostly occupied Ga $4p$ and empty Ga $4s$ states.

From this assignment, it can be inferred that transitions of mixed character involving Ga and S states result in the main peaks observed in the ϵ_2 spectrum corresponding to the intralayer covalent bonding of GaS, whereas anion S-states contributes mainly to the broad features in the range 4.2 to 5 eV, due to the vdW interaction between layers. This is supported by the second derivative analysis of the theoretical dielectric function for both polarizations, namely the intense CPs E_1 and E_5 appearing in the $d^2\epsilon_2/dE^2$ (probing parallel to the layer) while the E_2 , E_4 and E_6 mainly characterize the $d^2\epsilon_2/dE^2$ (probing along the c -axis and therefore interlayers).

In order to assess any thickness dependence of the dielectric function of GaS in the few-layer regime, different exfoliation runs of the same bulk crystal were executed. Spectroscopic imaging ellipsometry (SIE) measurements were performed on GaS flakes of different and known thicknesses down to few layers transferred onto a smooth sapphire substrate. Given the $\approx 1\mu\text{m}$ lateral resolution of SIE, spectroscopic ellipsometry spectra have been acquired in specific flakes of known and homogeneous thickness avoiding averaging effects between layers of different thicknesses. Figure 4(a) shows the ellipsometric enhanced contrast map of a typical GaS flake. The regions of interest (ROIs) where the dielectric function has been measured are indicated in green, and the corresponding ROIs optical micrograph and AFM topography are shown in Figs. 4(b),(c). The thickness of the layers in the ROIs is approximately 50 Å and 180 Å as measured by AFM line profiles. Those ROI GaS flakes measured by SIE, have been characterized structurally by Raman spectroscopy as reported in Fig. 5(e). The Raman spectra acquired in the ROIs present the characteristic A_{1g}^1 , E_{2g}^1 and A_{1g}^2 Raman modes of GaS [36] with preserved 1:1 ratio between the A_{1g}^1 and A_{1g}^2 modes characteristic of the $2H$ -polytype, as also supported by the main (002) and (004) reflections in the XRD pattern also show in Fig. 5.

Figure 4(d) shows the ellipsometric magnitudes of Ψ and Δ maps measured at the photon energy of 3.5 eV. The Ψ and Δ maps for additional photon energies are available in the data set Ref. [39]. From the Ψ and Δ maps (at the various photon energies) over the ROIs, and considering the thickness measured by the AFM profilometry, the dielectric function has also been determined for both the 50 Å (approximately 5 layers) and 180 Å (approximately 18 layers) thick GaS flakes as shown in Fig. 4(e). The ellipsometric fitting is shown in Fig. 4(f),(g) using a model as the one sketch as inset. Interestingly, the dielectric function for the 180 Å GaS flake overlaps with bulk GaS indicating that for already that number of layers, the $2H$ - bulk dielectric

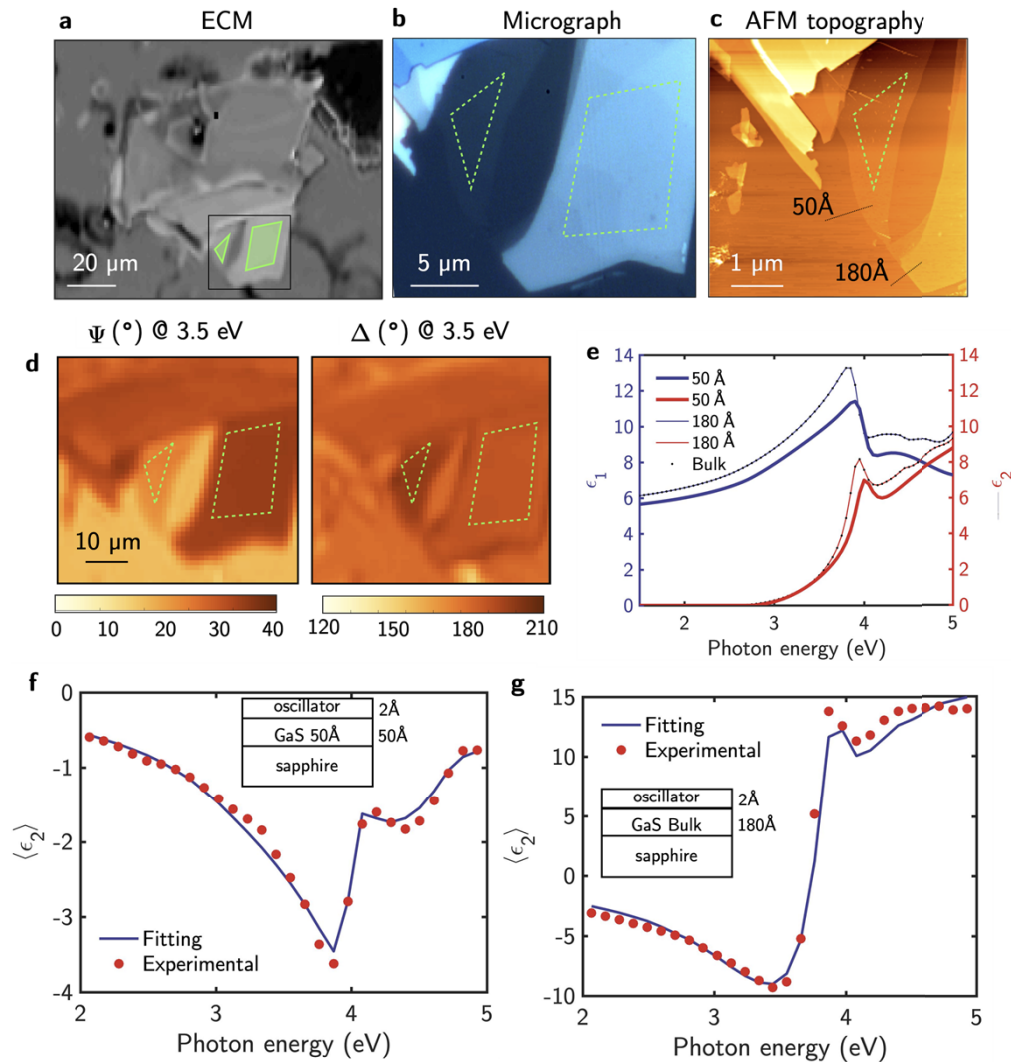


Fig. 4. (a) Ellipsometric enhanced contrast micrograph (ECM) of an exfoliated GaS flake on a sapphire substrate. The green regions (ROIs) indicate the area where the spectroscopic ellipsometry measurements have been performed. (b) Optical micrograph and (c) AFM topography images of the analyzed red regions. (d) Representative ellipsometric Ψ and Δ maps measured at the photon energy of 3.5 eV of the black square region indicated in (a). The green dashed contour in (d) indicates the homogeneous Ψ and Δ regions to extract the few layer dielectric function. (e) Real, ϵ_1 , and imaginary, ϵ_2 , parts of the dielectric function extracted for the 50 Å and 180 Å thick GaS flake, corresponding to approximately 5 layers and 18 layers, respectively. For comparison, the GaS bulk dielectric function is also plotted. Example of fitting quality for the experimental imaginary part of the pseudo dielectric of (f) 50 Å and (g) 180 Å thick exfoliated GaS layers using a layer-stack model as the ones sketched. The χ^2 of the fittings are 0.5 and 2.5 respectively.

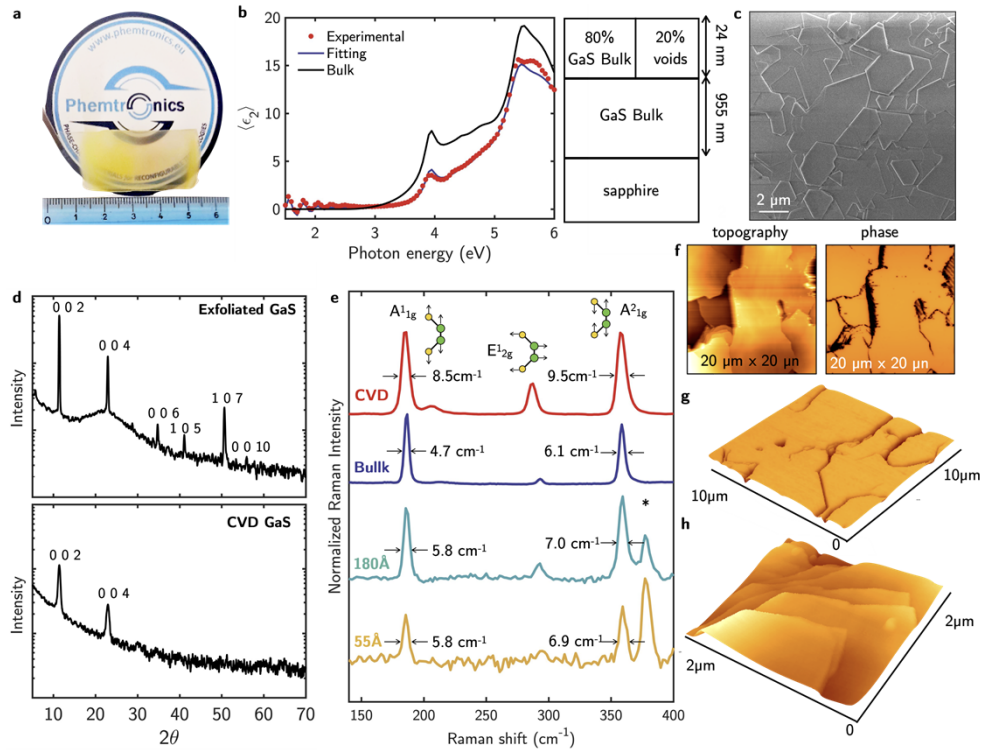


Fig. 5. (a) Picture of the cm-scale grown GaS on sapphire substrate. (b) Imaginary part, $\langle \epsilon_2 \rangle$, of the pseudo-dielectric function of a typical CVD grown GaS sample with a thickness of approximately $1\ \mu\text{m}$. The measured spectra have been fitted using the model sketched in (b). For comparison, the determined reference dielectric function of $2H$ -GaS is plotted (black-line). (c) Scanning electron microscopy image of the analyzed CVD GaS sample. (d) XRD spectra of exfoliated and CVD. (e) Raman spectra of bulk, $\sim 50\ \text{\AA}$ and $\sim 180\ \text{\AA}$ thick exfoliated GaS, and of $\sim 1\ \mu\text{m}$ CVD GaS. A sketch and labeling of the A_{1g}^1 , E_{2g}^1 and A_{1g}^2 GaS modes are included. The peak at $377\ \text{cm}^{-1}$ is due to the sapphire substrate (*) on which samples are deposited; the full width at half maximum (FWHM) is also given. (f-h) AFM images of the CVD sample: (f) topography and corresponding phase of CVD GaS crystals very homogeneous in phase evidencing grain boundaries; (g) 3D topography of the crystals with grain boundaries; (h) 3D topography of the CVD crystal boundary showing the layered structure of the CVD sample.

function applies also to few layers. Noteworthy, also for very few layers, namely monolayer to 5 layers, the dielectric function approaches that of bulk GaS, consistently with the in-plane component determining the dielectric function also of few layers GaS, independently of the number of layers. Indeed, with the decrease of the number of layers, an increase of the bandgap to 2.7 ± 0.5 eV for approximately 5 layers and to 3.1 ± 0.5 eV for monolayer is found in agreement with the trend revealed by the DFT calculations.

3.3. Optical properties of CVD grown crystalline GaS

We also demonstrate that the determined dielectric function can be applied to the analysis of CVD grown crystalline GaS samples with thicknesses ranging from few layers up to ≈ 1 μm . In order to qualify the CVD GaS, Fig. 5 shows a picture of the cm-scale grown GaS on sapphire substrate, with the XRD pattern showing only the (002) and (004) reflections demonstrating that our CVD GaS consists of crystals orientated perpendicular to the c -axis as in the case of the bulk $2H$ -crystal, whose layered structure can be seen in Fig. 5(h). The fact that only the most intense reflections could be seen for the CVD sample could be due to the misalignment of the stacked layers and to grain boundaries clearly visible in Figs. 5(f),(g). The size and planar coalescence of those crystals can be seen in the SEM picture in Fig. 5(c) as well as by AFM in Figs. 5(f),(g), with a grain surface roughness RMS (root mean square roughness) of 0.9 nm. The AFM images in Fig. 5(f) show the topography and phase of CVD GaS crystals very homogeneous in phase evidencing grain boundaries. The corresponding Raman spectrum, shown in Fig. 5(e), presents the characteristic A_{1g}^1 , E_{2g}^1 and A_{1g}^2 Raman modes of GaS, with the A_{1g}^1 and A_{1g}^2 modes preserving the 1:1 ratio wavenumber characteristic of a well ordered $2H$ - polytype. The full width at half maximum (FWHM) is also indicated.

The imaginary, $\langle \epsilon_2 \rangle$, part of the pseudodielectric function of CVD GaS is compared to the reference GaS dielectric function in Fig. 5(b), along with its fitting using the sketched model. Interestingly, the CVD GaS pseudodielectric function shows well shaped GaS CPs, with a lower amplitude, due to grain boundaries well visible in the SEM and AFM images. The pseudodielectric function of the CVD GaS has been fit with the optical model sketched in Fig. 5(b), consisting of bulk GaS (same dielectric function as in Fig. 3(a)) and a surface roughness layer modeled using a Bruggeman effective medium approximation of 80% bulk GaS and 20% voids. The quality of the fitting, also shown in Fig. 5(a), demonstrates that the established dielectric function for GaS can be used to model the optical response of the c -axis oriented CVD GaS layers, with the voids volume fraction giving an indication of the grain boundaries, and therefore of the coalescence and large size of grains.

4. Conclusions

We have reported, to the best of our knowledge, the first detailed experimental and theoretical analysis of the dielectric function of bulk and low-dimensional GaS down to monolayer obtained by both mechanical exfoliation and CVD. Noteworthy, the contribution of the in-plane dielectric function, which is mostly independent of number of layers, predominates. The critical points appearing in the dielectric function of GaS are identified in terms of location in the reciprocal space and atomic character of the states involved in the interband transitions. Hence, the main features in the optical response function of GaS were found to result from excitations of Ga $4p$ and S $3p$ to empty Ga $4s$ and $4p$ antibonding levels, corroborating the predominance of the intralayer bonds to the dielectric function, with a negligible contribution of the interlayer vdW interactions. The established dielectric function applies to the analysis of both exfoliated and CVD GaS and opens new paths to accurately model and design new optical devices based on GaS.

Funding. Horizon 2020 Framework Programme (No 899598 – PHEMTRONICS).

Disclosures. The authors declare no conflict of interests.

Data availability. Delta and Psi mas from imaging ellipsometry measurements are available at [39]. Dielectric function and refractive index of bulk GaS are available at [40].

References

1. T. Chen, Y. Lu, Y. Sheng, Y. Shu, X. Li, R.-J. Chang, H. Bhaskaran, and J. H. Warner, "Ultrathin All-2D Lateral Graphene/GaS/Graphene UV Photodetectors by Direct CVD Growth," *ACS Appl. Mater. Interfaces* **11**(51), 48172–48178 (2019).
2. C. S. Jung, F. Shojaei, K. Park, J. Y. Oh, H. S. Im, D. M. Jang, J. Park, and H. S. Kang, "Red-to-Ultraviolet Emission Tuning of Two-Dimensional Gallium Sulfide/Selenide," *ACS Nano* **9**(10), 9585–9593 (2015).
3. X. Li, L. Tao, Z. Chen, H. Fang, X. Li, X. Wang, J.-B. Xu, and H. Zhu, "Graphene and related two-dimensional materials: Structure-property relationships for electronics and optoelectronics," *Appl. Phys. Rev.* **4**(2), 021306 (2017).
4. A. Chaves, J. G. Azadani, H. Alsalman, D. R. da Costa, R. Frisenda, A. J. Chaves, S. H. Song, Y. D. Kim, D. He, J. Zhou, A. Castellanos-Gomez, F. M. Peeters, Z. Liu, C. L. Hinkle, S. H. Oh, P. D. Ye, S. J. Koester, Y. H. Lee, P. Avouris, X. Wang, and T. Low, "Bandgap engineering of two-dimensional semiconductor materials," *npj 2D Mater. Appl.* **4**(1), 29 (2020).
5. Z. Wang, M. Safdar, M. Mirza, K. Xu, Q. Wang, Y. Huang, F. Wang, X. Zhan, and J. He, "High-performance flexible photodetectors based on GaTe nanosheets," *Nanoscale* **7**(16), 7252–7258 (2015).
6. E. Mercado, Y. Zhou, Y. Xie, Q. Zhao, H. Cai, B. Chen, W. Jie, S. Tongay, T. Wang, and M. Kuball, "Passivation of Layered Gallium Telluride by Double Encapsulation with Graphene," *ACS Omega* **4**(19), 18002–18010 (2019).
7. S. G. Choi, D. H. Levi, C. Martinez-Tomas, and V. Muñoz Sanjosé, "Above-bandgap ordinary optical properties of GaSe single crystal," *J. Appl. Phys.* **106**(5), 053517 (2009).
8. J. L. Brebner and G. Fischer, "THE OPTICAL ABSORPTION EDGE OF GaS," *Can. J. Phys.* **41**(3), 561–563 (1963).
9. J. L. Brebner, "The optical absorption edge in layer structures," *J. Phys. Chem. Solids* **25**(12), 1427–1433 (1964).
10. E. Aulich, J. L. Brebner, and E. Mooser, "Indirect Energy Gap in GaSe and GaS," *Phys. status solidi* **31**(1), 129–131 (1969).
11. A. Cingolani, A. Minafra, P. Tantalo, and C. Paorici, "Edge emission in GaSe and GaS," *Phys. Status Solidi* **4**(1), K83–K85 (1971).
12. M. Grandolfo, F. Somma, and P. Vecchia, "Temperature Modulation of the Optical Constants of Layer Compounds GaSe and GaS," *Phys. Rev. B* **5**(2), 428–434 (1972).
13. S. Adachi and C. Hamaguchi, "Resonant Brillouin Scattering in GaSe and GaS," *J. Phys. Soc. Japan* **48**(6), 1981–1989 (1980).
14. H. L. Zhuang and R. G. Hennig, "Single-Layer Group-III Monochalcogenide Photocatalysts for Water Splitting," *Chem. Mater.* **25**(15), 3232–3238 (2013).
15. Y. Bai, K. Deng, and E. Kan, "Band gap engineering and visible light response for GaS monolayer by isovalent anion-cation codoping," *Mater. Chem. Phys.* **198**, 275–282 (2017).
16. S. Zhou, C.-C. Liu, J. Zhao, and Y. Yao, "Monolayer group-III monochalcogenides by oxygen functionalization: a promising class of two-dimensional topological insulators," *npj Quantum Mater.* **3**(1), 16 (2018).
17. D. J. Late, B. Liu, J. Luo, A. Yan, H. S. S. R. Matte, M. Grayson, C. N. R. Rao, and V. P. Dravid, "GaS and GaSe Ultrathin Layer Transistors," *Adv. Mater.* **24**(26), 3549–3554 (2012).
18. Y. Lu, J. Chen, T. Chen, Y. Shu, R. Chang, Y. Sheng, V. Shautsova, N. Mkhize, P. Holdway, H. Bhaskaran, and J. H. Warner, "Controlling Defects in Continuous 2D GaS Films for High-Performance Wavelength-Tunable UV-Discriminating Photodetectors," *Adv. Mater.* **32**(7), 1906958 (2020).
19. Y. Lu, T. Chen, N. Mkhize, R.-J. Chang, Y. Sheng, P. Holdway, H. Bhaskaran, and J. H. Warner, "GaS:WS 2 Heterojunctions for Ultrathin Two-Dimensional Photodetectors with Large Linear Dynamic Range across Broad Wavelengths," *ACS Nano* *acs.nano.1c06587* (2021).
20. W. Zhong, Y. Liu, X. Yang, C. Wang, W. Xin, Y. Li, W. Liu, and H. Xu, "Suspended few-layer GaS photodetector with sensitive fast response," *Mater. Des.* **212**, 110233 (2021).
21. S. Dicatorato, Y. Gutiérrez, M. M. Giangregorio, F. Palumbo, G. V. Bianco, and M. Losurdo, "Interplay between Thickness, Defects, Optical Properties, and Photoconductivity at the Centimeter Scale in Layered GaS," *Nanomaterials* **12**(3), 465 (2022).
22. A. Harvey, C. Backes, Z. Gholamvand, D. Hanlon, D. McAteer, H. C. Nerl, E. McGuire, A. Seral-Ascaso, Q. M. Ramasse, N. McEvoy, S. Winters, N. C. Berner, D. McCloskey, J. F. Donegan, G. S. Duesberg, V. Nicolosi, and J. N. Coleman, "Preparation of Gallium Sulfide Nanosheets by Liquid Exfoliation and Their Application As Hydrogen Evolution Catalysts," *Chem. Mater.* **27**(9), 3483–3493 (2015).
23. P. Hu, L. Wang, M. Yoon, J. Zhang, W. Feng, X. Wang, Z. Wen, J. C. Idrobo, Y. Miyamoto, D. B. Geohegan, and K. Xiao, "Highly Responsive Ultrathin GaS Nanosheet Photodetectors on Rigid and Flexible Substrates," *Nano Lett.* **13**(4), 1649–1654 (2013).
24. M. I. Zappia, G. Bianca, S. Bellani, N. Curreli, Z. Sofer, M. Serri, L. Najafi, M. Piccinni, R. Oropesa-Núñez, P. Marvan, V. Pellegrini, I. Kriegel, M. Prato, A. Cupolillo, and F. Bonaccorso, "Two-Dimensional Gallium Sulfide Nanoflakes for UV-Selective Photoelectrochemical-type Photodetectors," *J. Phys. Chem. C* **125**(22), 11857–11866 (2021).

25. M. Isik, N. M. Gasanly, and R. Turan, "Interband transitions in gallium sulfide layered single crystals by ellipsometry measurements," *Phys. B Condens. Matter* **408**(1), 43–45 (2013).
26. Y. Gutiérrez, M. M. Giangregorio, S. Dicorato, F. Palumbo, and M. Losurdo, "Exploring the Thickness-Dependence of the Properties of Layered Gallium Sulfide," *Front. Chem.* **9**, (2021).
27. J. M. Soler, E. Artacho, J. D. Gale, A. García, J. Junquera, P. Ordejón, and D. Sánchez-Portal, "The SIESTA method for ab initio order-*N* materials simulation," *J. Phys. Condens. Matter* **14**(11), 2745–2779 (2002).
28. J. P. Perdew, A. Ruzsinszky, G. I. Csonka, O. A. Vydrov, G. E. Scuseria, L. A. Constantin, X. Zhou, and K. Burke, "Restoring the Density-Gradient Expansion for Exchange in Solids and Surfaces," *Phys. Rev. Lett.* **100**(13), 136406 (2008).
29. D. R. Hamann, "Optimized norm-conserving Vanderbilt pseudopotentials," *Phys. Rev. B* **88**(8), 085117 (2013).
30. M. J. van Setten, M. Giantomassi, E. Bousquet, M. J. Verstraete, D. R. Hamann, X. Gonze, and G.-M. Rignanese, "The PseudoDojo: Training and grading a 85 element optimized norm-conserving pseudopotential table," *Comput. Phys. Commun.* **226**(3), 39–54 (2018).
31. H. J. Monkhorst and J. D. Pack, "Special points for Brillouin-zone integrations," *Phys. Rev. B* **13**(12), 5188–5192 (1976).
32. S. Yang, Y. Li, X. Wang, N. Huo, J.-B. Xia, S.-S. Li, and J. Li, "High performance few-layer GaS photodetector and its unique photo-response in different gas environments," *Nanoscale* **6**(5), 2582–2587 (2014).
33. V. Zólyomi, N. D. Drummond, and V. I. Fal'ko, "Band structure and optical transitions in atomic layers of hexagonal gallium chalcogenides," *Phys. Rev. B* **87**(19), 195403 (2013).
34. D. V. Rybkovskiy, A. V. Osadchy, and E. D. Obraztsova, "Transition from parabolic to ring-shaped valence band maximum in few-layer GaS, GaSe, and InSe," *Phys. Rev. B* **90**(23), 235302 (2014).
35. D. M. Hoat, "Comparative study of structural, electronic, optical and thermoelectric properties of GaS bulk and monolayer," *Philos. Mag.* **99**(6), 736–751 (2019).
36. M. J. Taylor, "Raman and infrared spectra and vibrational assignments of gallium (II) sulphide," *J. Raman Spectrosc.* **1**(4), 355–358 (1973).
37. M. Schlüter, J. Camassel, S. Kohn, J. P. Voitchovsky, Y. R. Shen, and M. L. Cohen, "Optical properties of GaSe and GaSxSe1-x mixed crystals," *Phys. Rev. B* **13**(8), 3534–3547 (1976).
38. A. Savitzky and M. J. E. Golay, "Smoothing and Differentiation of Data by Simplified Least Squares Procedures," *Anal. Chem.* **36**(8), 1627–1639 (1964).
39. Y. Gutierrez, D. Juan, S. Dicorato, G. Santos, M. Duwe, P. Thiesen, M. M. Giangregorio, F. Palumbo, K. Hingerl, C. Cobet, P. Garcia-Fernandez, J. Junquera, F. Moreno, and M. Losurdo, "Data Set - Imaging ellipsometry on exfoliated GaS on sapphire substrate," Zenodo: Version 1, 10 February (2022), <https://doi.org/10.5281/zenodo.6034897>.
40. Y. Gutierrez, D. Juan, S. Dicorato, G. Santos, M. Duwe, P. Thiesen, M. M. Giangregorio, F. Palumbo, K. Hingerl, C. Cobet, P. Garcia-Fernandez, J. Junquera, F. Moreno, and M. Losurdo, "Data Set - Dielectric function crystalline 2H-GaS," Zenodo: Version 1, 2 June (2022), <https://doi.org/10.5281/zenodo.6607596>.